Beyond Cross-Modal Alignment: Measuring and Leveraging Modality Gap in Vision-Language Models

Anonymous ACL submission

Abstract

The success of vision-language models is primarily attributed to effective cross-modal alignment between vision and language. However, modality gaps persist even in well-aligned models and may be necessary for human perception, as evidenced by modality-specific phenomena such as visual texture and linguistic tone. These observations motivate us to computationally measure and leverage modality gaps to explore their utility in downstream applications. In this paper, we introduce the **M**odality **D**ominance **S**core (**MDS**), which attributes multimodal features to specific modalities by categorizing them as vision-dominant, language-dominant, or cross-modal. We then propose automatic interpretability metrics to evaluate these modality-specific features in a scalable manner. Finally, we demonstrate how the identified modality-specific features enable training-free probing and editing methods for understanding model perception across genders, generating adversarial examples, and controlling text-to-image generation. Combined with task-agnostic interpretability tools, our work provides a systematic framework for analyzing and efficiently controlling multimodal models.

1 Introduction

Multimodal Models (MMs) have become foundational to the advancement of AI, enabling systems to process and understand information from multiple data modalities, such as vision and language (Radford et al., 2021; Kim et al., 2021; Lu et al., 2019; Liang et al., 2024). Vision-Language Models (VLMs), a prominent class of MMs, operate under the premise that different data modalities share common, or cross-modal, features that can be jointly learned (Ngiam et al., 2011; Sun et al., 2024; Li et al., 2025).

Alongside these remarkable advancements, ongoing research aims to deepen our understanding of how different modalities interact and diverge within MMs (Liang et al., 2022; Rawal et al., 2023; Schrodi et al., 2025; Zhang et al., 2025). For instance, Liang et al. (2022) revealed the modality gap as a geometric phenomenon in which image and text embeddings reside in disjoint regions of the shared embedding space. Zhang et al. (2025) proposed the MC^2 benchmark and identified clear modality bias across 18 tested large VLMs. Researchers have also developed automatic measurement methods (Liang et al., 2022; Rawal et al., 2023; Parcalabescu and Frank, 2023, 2025) and optimization techniques to calibrate modality gaps (Rawal et al., 2023; Zhang et al., 2024).

Despite these measurement and optimization methods, existing studies treat modality gaps as undesirable imperfections—primarily diagnosing model collapse (Rawal et al., 2023; Zhang et al., 2024; Schrodi et al., 2025; Parcalabescu and Frank, 2025) or motivating new training algorithms for improved alignment. Our work takes a different perspective: we posit that *modality gaps are both prevalent and beneficial for downstream tasks*. This perspective is grounded in cognitive science, where modality commonality and separation have long been central themes. Paivio (1991); Spence (2011); Fan et al. (2016) have examined how humans integrate and differentiate information across sensory modalities, suggesting that modal specificity may be functionally advantageous rather than merely an artifact of imperfect alignment.

To investigate this hypothesis in VLMs, we conduct a systematic study with three contributions:

1. We demonstrate that modality-specific information can be extracted from VLMs—specifically, text-dominant (`TextD`), image-dominant (`ImgD`), and cross-modal (`CrossD`) features—and show that these features exhibit distinct activation patterns when processing images versus text.

2. We propose embedding-based interpretability metrics to measure monosemanticity (within-modality coherence) and modality fidelity (cross-modality validation) in a multimodal setting.

These metrics are scalable and compatible with existing top-k activated interpretations.

3. We design lightweight probing and steering methods to analyze models' perception and demonstrate how modality-specific features enable control over VLM behavior in tasks such as bias analysis, adversarial example generation, and text-to-image generation.

2 Related Work

Modality Gap. Researchers have identified that modality bias and gaps are prevalent in both early VLMs (Liang et al., 2022) and large VLMs (Zhang et al., 2025). Moreover, modality gaps have been shown to negatively impact downstream tasks such as video understanding (Rawal et al., 2023) and object detection (Schrodi et al., 2025). Several metrics have been proposed to quantify modality gaps, including geometry-based methods such as L2M (Liang et al., 2022) and RGM (Schrodi et al., 2025), as well as Shapley-value-based approaches (Parcalabescu and Frank, 2023, 2025), which measure the degree to which individual modalities contribute to model predictions. *Our work differs in two key aspects:* (i) we measure modality gaps at the feature level, identifying how individual features respond differentially to different modalities; (ii) we leverage modality-specific features for probing and steering, treating modality specialization as a functional asset rather than an imperfection.

Interpretability Measurements. Existing interpretability measurements are based on summarizing patterns in top-k activated samples. For example, logit lens (nostalgebraist, 2020) has inspired many studies in both unimodal and multimodal representation understanding (Parekh et al., 2024; Jiang et al., 2025). The embedding-based extension (Phukan et al., 2025) alleviates its limitation in processing contextual-related concepts. More recently, LLMs have been used to generate explanations for activation patterns, with prediction accuracy on held-out samples serving as an interpretability proxy (Bills et al., 2023). However, this LLM-as-a-judge approach is computationally expensive and only measures semantic coherence within the unimodality, neglecting cross-modality consistency. *Our interpretability metrics address these limitations* through scalable embedding-based computation and introduce modality fidelity to fill the gap.

3 Identify Modality-Specific Features

Cross-modal alignment is important for VLMs, yet modality gaps remain a widely observed phenomenon (Liang et al., 2022; Schrodi et al., 2025). Liang et al. (2022); Schrodi et al. (2025) attributed this to geometric characteristics of the representation space; notably, Schrodi et al. (2025) observed that modality bias can be traced to a few embedding dimensions. Focusing on the representation space as well, we go further by attributing each dimension to a specific modality dominance class—text-dominant, image-dominant, or cross-modal—enabling fine-grained analysis and control.

Background: Modality Alignment in VLMs. Typically, there are an image encoder and a text encoder in a VLM for image and text input processing, respectively. Specifically, the image-text pair $(x_{\text{img}}, x_{\text{txt}})$ is fed to an image encoder f_{img} and a text encoder f_{txt} within the model, respectively and the final-layer representations $z_{\text{img}} \in \mathbb{R}^D$ and $z_{\text{txt}} \in \mathbb{R}^D$ are then optimized jointly in the shared D-dimensional representation space. An alignment loss, such as the contrastive loss in CLIP (Ilharco et al., 2021) across the two modalities, is applied for modality alignment.

3.1 Modality-specific Feature Identification

To measure the modality gap, Liang et al. (2022) used the difference between the center of image embeddings and text embeddings of M input pairs, i.e., $\frac{1}{M}(\sum_{i=1}^{M} ||z_{\text{img},i}||_2 - \sum_{i=1}^{M} ||z_{\text{txt},i}||_2)$. We extend this model-level measurement to a fine-grained metric, i.e., the predominant modality associated with each dimension $d \in \{1, 2, \ldots, D\}$ in the shared embedding space. The proposed modality dominance score (**MDS**), denoted as $R(d)$ shown in Eq. (1) reflects how strongly the d-th feature [1] is influenced by the image modality:

$$R(d) = \frac{1}{M} \sum_{i=1}^{M} \frac{||z_{\text{img},i}^{(d)}||}{||z_{\text{img},i}^{(d)}|| + ||z_{\text{txt},i}^{(d)}||}. \quad (1)$$

Specifically, we feed M image-text pairs to the VLM and extract the corresponding image features $z_{\text{img},i}$ and text features $z_{\text{txt},i}$ for i-th input. For each d-th dimension in the D-dimension shared space, we calculate the relative activation between the features from the two modalities. This modality fraction is averaged over more than $M = 10k$

[1] Each feature dimension corresponds directly to a neuron in the VLM's final layer; our study thus focuses on the interpretability of the model's intrinsic components.

input pairs, providing a representative estimate of the modality distribution. Implementation details are in Appendix A.1.

We then categorize all D features into three groups based on their deviation from the mean μ and standard deviation σ of the MDS distribution:

$$\texttt{TextD}: \; R(d) < \mu - \sigma;$$
$$\texttt{CrossD}: \; \mu - \sigma < R(d) < \mu + \sigma;$$
$$\texttt{ImgD}: \; R(d) > \mu + \sigma$$

We anticipate that ImgD features are predominantly activated by visual concepts, TextD features by textual concepts, and CrossD features are simultaneously activated by the shared commonalities. This modality fidelity will be evaluated in §4.2.

3.2 Quantitative Evaluation for MDS

To verify that modality-specific features effectively capture their intended modality information, we employ an intervention-based evaluation. Specifically, we remove these features from the original CLIP ViT-H/14 (LAION-2B) (Ilharco et al., 2021) representation by zeroing out their corresponding indices, then use the modified representations as input to a logistic regression classifier. We evaluate performance on image and text classification tasks using samples from COCO (Lin et al., 2014). A decrease in classification accuracy indicates that the removed features contained substantial modality-specific information, thereby validating our feature attribution method.

The results are shown in Table 1. It is observed that removing the ImgD features leads to larger classification degradation in image classification, while removing TextD leads to larger drops in text classification; while CrossD does not show any particular modality tendency in classification.

3.3 Qualitative Evaluation for MDS

We randomly select features from the three groups, and then display their most-activated images and texts in Figure 1 (ImD), Figure 2 (TextD), and Figure A1 (CrossD). **ImgD activates fundamental visual concepts, such as repeated patterns and colors.** Feature 647 activates images with diverse repetitive patterns; feature 667 focuses on scenes with aquatic-blue elements. Although less coherent than the images, some patterns do emerge for its activated texts: feature-647 activates two sentences that refer to repetitive patterns, such as "*tufted upholstery*"; feature-667 activates texts related to "*snowy*" and "*winter*". These observations indicate

Task	Remove	# Features	Accuracy	Δ Acc
Image CLS	None	0	**0.776**	/
	Random	426	0.757	-2.1%
	ImgD	426	**0.750**	**-2.6%**
	Random	554	0.756	-2.0%
	TextD	554	0.760	-1.0%
	Random	44	0.773	-0.3%
	CrossD	44	0.769	-0.5%
Text CLS	None	0	**0.713**	/
	Random	426	0.694	-1.9%
	ImgD	426	0.702	-1.1%
	Random	554	0.693	-2.0%
	TextD	554	**0.683**	**-3.0%**
	Random	44	0.710	-0.3%
	CrossD	44	**0.712**	-0.1%

Table 1: Performance of modality-specific classification (CLS) after removing: random vs. specialized features, i.e., ImgD, TextD and CrossD. We also remove the same number of random feature indices for comparison.

the modality alignment, while the visual commonalities are more predominant for the ImgD. **TextD capture abstract concepts, such as human feelings and atmosphere.** For the activated images for feature-34 (the 1st row), most of the images have red color, with one image depicting a couple talking beside the sea; for feature-242, there are no clear patterns among the activated images. When looking at the activated texts, sentences activated by feature-34 center around a sweet and happy atmosphere between couples, with themes like cuddling, embracing, and hugging. Feature-242 focuses on strong human emotions, such as "*never*", "*terrifying*" and exclamation marks. These TextD generally correspond to abstract and consistent human emotions, which can be conveyed with a variety of visual objects. For example, in the second row, the first image depicts a collection of stones forming a heart shape, while the fourth image is a scenic view during a great trip. **CrossD (the majority features) capture shared semantics across modalities.** Differently, CrossD features capture common concepts that could be expressed in both visual and language modalities. Details can be found in § A.2.

4 Automatic Interpretability Evaluation

Although we have identified modality-dominant features, features in deep models are inherently *polysemantic* (Olah et al., 2020)—each feature often encodes multiple unrelated semantic concepts, potentially spanning both textual and visual modalities, which hinders interpretability. *Monosemanticity* (Elhage et al.; Bills et al., 2023; Gurnee et al.,

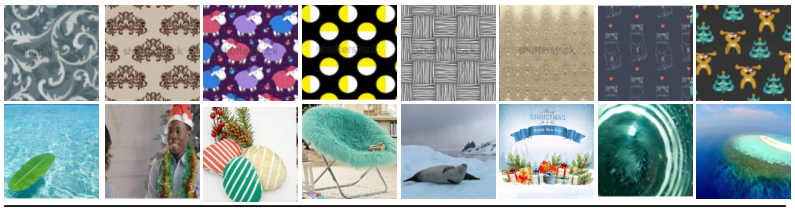

Feature-647: Pattern and others.	*Feature-667: Scenes in winter and other.*
A bed with tufted upholstery.	White trotting on snowy ground with a tree.
Seamless pattern, flowers on a background.	Covering the trailhead in a winter wonderland.
Could new showroom and model signal the start?	The image of drum under the white background.

Figure 1: Activated images and texts (in Table) by `ImgD`. Top image row (feature 647): patterns and textures. Bottom image (feature 667): water and aquatic themes in blue. Texts in blue align with visual concepts.

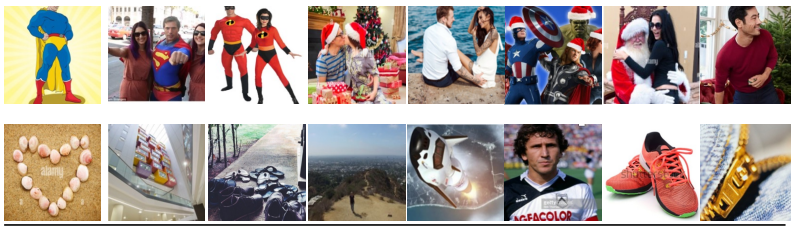

Feature-34: Sweet and happy Couple.	*Feature-242: Strong emotion.*
Attractive young couple sitting on a bench, talking and laughing with the city.	Animal looking for a cat tree without carpet your options have greatly expanded.
Sculpture of lovers at the temple	Sinkhole, most terrifying thing I have ever seen.
Young couple in love, hugging in the old part of town.	We're away from the beginning of the holiday season here!

Figure 2: Activated images and texts (in Table) by `TextD`. Top image row (feature 34): couples and individuals in red attire. Bottom image row (feature 242): diverse objects. Text in blue aligns with visual concepts.

2023; Yan et al., 2024) has thus emerged as a paradigm for deriving interpretable features that encode single, coherent concepts. However, scaling interpretability evaluation remains an open challenge due to the heavy reliance on costly human annotations (Gao et al., 2024) or LLM explanations (Bills et al., 2023). To address this bottleneck, we propose a suite of automated metrics to measure feature interpretability.

4.1 Overview

Top-k activation-based interpretation. A feature is considered interpretable if its semantic meaning can be readily understood by humans. In practice, interpretability is assessed by examining whether the top-k most highly activated samples exhibit coherent and consistent patterns—a standard approach for analyzing both language (Geva et al., 2021) and multimodal models (Parekh et al., 2024). To incorporate semantic similarity, Bills et al. (2023) extended this approach by computing the correlation between predicted activation values (based on explanations of the top-k samples) and true activations. This correlation-based method relaxes the hard constraint of requiring perfect pattern consistency across top-k samples.

Building upon the *"soft"* top-k activation framework, we propose scalable, *embedding-based* evaluation metrics tailored to multimodal models. In this context, interpretability encompasses two dimensions:

- ***Monosemanticity*** (within-modality coherence). It measures whether a feature's top-k activated samples exhibit semantic coherence within a single modality based on their embedding similarity.
- ***Modality fidelity*** (cross-modality validation). It compares the monosemanticity scores across modality-attributed features to assess whether features remain faithful to their assigned modality. For example, when processing visual inputs, `ImgD` should exhibit higher monosemanticity scores than `TextD`, and vice versa for textual inputs.

4.2 Intepretability Metrics

Given a feature $z^{(d)}$, the d-th dimension of $z \in \mathbb{R}^D$, we propose to use embedding models $h : \mathbb{Z}^D \to \mathbb{Z}^{D'}$ to calculate the interpretability metrics.

Monosemanticity. For each image/text feature $z^{(d)}$, we collect the top m most-activated image/-text samples for this dimension, and feed them to the embedding model h to get $Z_+ \in \mathbb{R}^{m \times D'}$. For comparison, we embed m random samples into

$Z_- \in \mathbb{R}^{m \times d'}$. Then, we calculate the inter-sample similarity between the selected samples, $S_+ = Z_+ Z_+^\top \in \mathbb{R}^{m \times m}$ and $S_- = Z_- Z_-^\top \in \mathbb{R}^{m \times m}$. The monosemanticity of an individual feature $z^{(d)}$ is measured by calculating the relative difference between the two similarity scores, denoted as $I(z^{(d)})$ (***EmbSim***). We also propose a binary metric to avoid the different scales in different modalities, denoted as $W(z^{(d)})$ (***WinRate***):

$$I(z^{(d)}) = \frac{1}{m(m-1)} \sum_{i \neq j} \frac{(S_+)_{ij} - (S_-)_{ij}}{(S_-)_{ij}},$$
$$W(z^{(d)}) = \frac{1}{m(m-1)} \sum_{i \neq j} \mathbf{1}_{[(S_+)_{ij} > (S_-)_{ij}]}.$$

The overall interpretability score is the average across all d dimensions for $z^{(d)}$ where $d \in [1, D]$. A higher monosemanticity score (both *EmbSim* and *WinRate* are ***Mono***, with a superscript representing the input modality) indicates that the extracted features exhibit stronger semantic consistency towards the given modality. [2]

Modality Fidelity. Based on the single-modality monosemanticity (semantic coherence), we proceed to cross-modality interpretability. Specifically, we ask: is `ImgD` indeed more effective at capturing coherent visual inputs than `TextD`? Similarly, is `TextD` better at encoding textual semantics compared to `ImgD`? Therefore, we define the modality fidelity as:

$$\textit{Visual Fidelity} = \textit{Mono}^{\text{vis}}(\texttt{ImgD}) - \textit{Mono}^{\text{vis}}(\texttt{TextD})$$
$$\textit{Textual Fidelity} = \textit{Mono}^{\text{txt}}(\texttt{TextD}) - \textit{Mono}^{\text{txt}}(\texttt{ImgD})$$

4.3 Interpretability Evaluation

Sparse Autoencoders (SAEs) (Cunningham et al., 2023) have been shown to effectively produce monosemantic features by enforcing sparsity constraints. To validate our evaluation framework, we apply our metrics to compare CLIP with and without SAE, expecting results consistent with existing literature on SAE's interpretability benefits. Beyond this validation, we also investigate whether other representation learning methods can enhance feature interpretability.

4.3.1 Comparison Models

We incorporate several representation learning algorithms that aim to learn modality-specific features. Implementation details are provided in § A.3.

[2] We calculate the average of *EmbSim* and *WinRate* as *Mono* in the main content; the separate results for the two metrics can be found in § A.4.2.

Multimodal SAEs. SAEs have emerged as a scalable tool for transforming polysemantic features into interpretable, monosemantic ones across different LLMs (Templeton, 2024; Gao et al., 2024; Lieberum et al., 2024). We extend it for VLMs by training a *single* SAE model $g : \mathbb{Z} \to \mathbb{Z}$ to reconstruct z, i.e., the final-layer outputs from the image and text encoder within CLIP, respectively. Specifically, we adopt that applies a linear encoder W_{enc} followed by a $\operatorname{Top} K$ operation that only keeps the K most activated units while zeroing out the rest. The sparse latent representation z^{sae} is then reconstructed using a linear decoder W_{dec}:

$$\begin{aligned} z^{\text{sae}} &= \operatorname{TopK}\left(W_{\text{enc}}\left(z - b_{\text{pre}}\right)\right), \\ \hat{z} &= W_{\text{dec}} z^{\text{sae}} + b_{\text{pre}}. \end{aligned} \tag{2}$$

$z \in \mathbb{R}^D$ is the inputs of SAE, i.e., z_{img} or z_{txt}. $z^{\text{sae}} \in \mathbb{R}^n$ is the learned sparse representation. We train the multimodal SAE to reconstruct z_i, z_t.

DeCLIP. Beyond multimodal supervision (image-text pairs), DeCLIP (Li et al., 2022) also incorporates single-modal self-supervision (image-image pairs and text-text) for more efficient joint learning.

Multimodal NCL. As shown in Wang et al. (2024), the non-negative constraints allow Non-negative Contrastive Learning (NCL) to extract highly sparse features and significantly improve feature monosemanticity. Therefore, we introduce a variant of NCL to enhance modality specification with the following loss,

$$-\mathbb{E}_{z_{\text{img}}, z_{\text{txt}}} \log \frac{\exp(g(z_{\text{img}})^\top g(z_{\text{txt}}))}{E_{z_{\text{txt}}^-} \exp(g(z_{\text{img}})^\top g(z_{\text{txt}}^-))}, \tag{3}$$

where here we use a ReLU-activated MLP network g to map input features to *non-negative* outputs.

4.3.2 Evaluation Results

Results of Monosemanticity. We compute the *Mono* score by identifying the top-20 most activated images and texts for each feature, respectively. From the average interpretability results in Figure 4, we observe the following: (i) *The features extracted using SAE and NCL (both enforce the feature sparsity) exhibit the highest overall monosemanticity* for both activated input images and texts. (ii) DeCLIP does not enhance interpretability through self-supervision alone; the monosemanticity on the textual side becomes even worse. This suggests that polysemantic features remain prevalent in DeCLIP.

Moreover, we observe that **monosemanticity enhancement encourages more modality-specific**

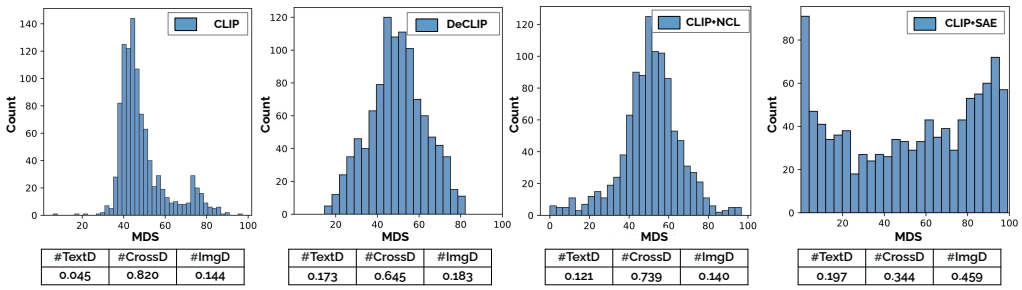

Figure 3: Modality Dominance Score (MDS) distributions of three feature categories for different VLMs.

neurons in Figure 3. The figure shows the MDS distributions across CLIP and other variants. CLIP contains a spectrum of features with different modality dominance, with its distribution skewed towards the image modality, and this trend is consistent across all models. DeCLIP, on the other hand, shows a more balanced and less centered distribution. This suggests that DeCLIP, through self-supervision, extracts more modality-specific features, which might be overlooked by pure vision-language contrastive models like CLIP. The extracted features on top of NCL and SAE also exhibit less skewness, *with SAE showing the most balanced distribution, indicating its strong capability to extract diverse monosemantic features.*

Results of Modality Fidelity. We have the following observations from Figure 5: (i) For CLIP, all the modality monosemanticity is negative, demonstrating the high entanglement of the two modality information. (ii) All the methods prompt the modality monosemanticity compared with CLIP. Particularly, the improvements of DeCLIP can be attributed to its single-modal alignment training loss, which could weaken some cross-modal associations in CLIP. (iii) NCL stands out as the best model for capturing both visual and textual monosemantic features, followed by SAE.

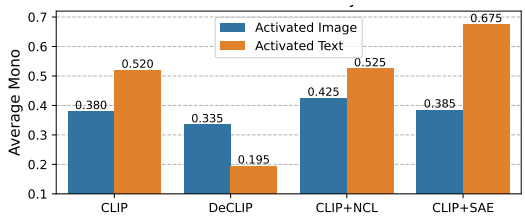

Figure 4: Monosemanticity.

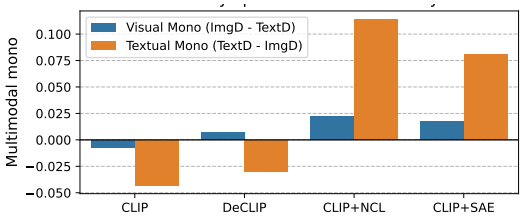

Figure 5: Modality Fidelity.

5 Leveraging the Modality Gap

Beyond interpretability, we design lightweight probing and steering methods based on modality-specific features to analyze VLMs' perceptual prreferences and enable precise behavioral control. Implementation details are in § A.5.

5.1 Understanding Gender Patterns

Gender is represented using both visual and textual features, and these data are used to train VLMs. To examine whether gender exhibits modality-specific representations, we investigate whether feminine concepts are more frequently conveyed through visual cues (e.g, via more colorful clothing) than through textual descriptions.

To answer this question, we collect both male and female images with their corresponding textual descriptions from the cc3m-wds (Sharma et al., 2018). These images are then encoded using the Clip+SAE model, extracting 1024-dimensional features for both female and male subjects. Next, we apply a zero-mask intervene strategy to remove the `ImgD` and `TextD` from these representations.

Gender	w/o ImgD	w/o TextD
Female	**17.65**	7.27
Male	5.64	**28.67**

Table 2: Gender classification changes (%) after removing `ImgD`(`textD`) **from input image(text)** for both female and male concepts identification. It is to verify the dominant modality for different genders.

We compare changes in gender classification accuracy when removing `ImgD` features from image inputs, which capture dominant feminine visual cues, versus removing `TextD` features from text inputs. As shown in Table 2, we find that feminine concepts are primarily preserved in `ImgD` (as the removal of `ImgD` from the image leads to larger classification degradation), whereas male concepts are more affected by the removal of `TextD`.

We sample female images that differ in the proportion of their most activated features categorized as `ImgD` features. The results are shown in Figure 6. From left to right, the fraction of activated `ImgD` features increases, and the images exhibit progressively more (*stereotypically*) feminine visual details, such as a backless skirt and hair accessories. The middle images show professional women, such as a doctor; while the leftmost image shows only a pair of legs in sports shoes, with minimal feminine cues aside from the pink color.

Figure 6: ***Female*** figures ordered by increasing percentages of `ImgD` (0.14, 0.16, 0.18, 0.20, 0.22, 0.24), corresponding to more feminine visual concepts.

5.2 Defense against Adversarial Attacks

We investigate the impact of different types of features on multimodal adversarial attacks (Cui et al., 2024; Yin et al., 2024), following the setup in Shayegani et al. (2024).

An adversarial sample is a benign-appearing image (e.g., a landscape) injected with harmful semantic content, such as the phrase *"I want to make a bomb"*. One defense-oriented optimization strategy involves minimizing the distance between the embeddings of an adversarial sample, $\mathbf{F}_{adv}$, and a paired benign sample, $\mathbf{F}_{ben}$, by updating the features in the adversarial sample (in Figure 7). The paired benign image is injected with a friendly phrase, such as *"peace and love"*.

To isolate the effects of our identified modality-specific features, we restrict alignment training to a selected set of feature indices I, corresponding to`ImgD`, `TextD`, and `CrossD`. The alignment loss is defined as $\mathcal{L} = \|\mathbf{F}_{adv}[:, I] - \mathbf{F}_{ben}[:, I]\|_2$. The optimized adversarial sample is then used to attack a VLM, LLaVA-1.5-7b (Liu et al., 2023). We evaluate the VLM's responses using an LLM-as-a-Judge framework, where DeepSeek-V3 (DeepSeek-AI et al., 2024) produces a binary label indicating attack success. We hypothesize that feature subsets encoding richer malicious semantics contribute most strongly to effective adversarial defense.

Results. The attack success rates are shown in Table 3. For alignment training, we select an equal number of features from `ImgD`, `TextD`, and `CrossD`, and additionally include a baseline that randomly

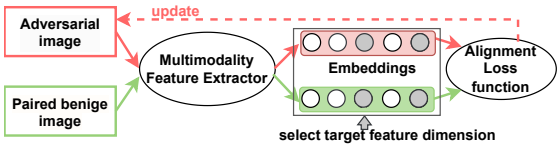

Figure 7: Alignment training to de-toxicity of the adversarial sample, with only selected target feature dimensions (in gray), i.e., `ImgD`, `TextD` and `CrossD` involved.

samples the same number of features from the union of all feature sets. Each adversarial sample is used to attack the VLM 100 times, and we generate a total of 50 adversarial samples. We observe that (i) compared with the original adversarial samples, alignment training using any subset of selected features reduces the attack success rate, indicating that feature-level alignment provides a degree of defense; (ii) using `TextD` yields the best defense performance, followed by `CrossD` and `ImgD`. This ordering is consistent with the nature of the attack, as the injected adversarial content primarily arises from harmful textual semantics. **These results demonstrate that `TextD` features effectively capture most of the semantic content relevant to the attack.** In contrast, `CrossD` captures only partial semantic information, while `ImgD` is least correlated with semantic information, resulting in minimal benefits for such modality-specific jailbreak defense.

Target feature	`ImgD`	`TextD`	`CrossD`
Success Rate (↓)	62.71%	24.89%	35.44%

Table 3: Success rate for adversarial attacks with different target features involved in the de-toxicity training. The success rate for original adversarial samples without alignment training is 73.26%, while for randomly selected features is 54.28%.

5.3 Controllable Text-to-Image Generation

Despite the impressive capabilities of text-to-image generation models (Koh et al., 2024; Swamy et al., 2024), their internal mechanisms for translating linguistic semantics into visual details remain poorly understood. A key challenge lies in disentangling the roles of modality-specific features in shaping generation fidelity and controllability. To address this, we conduct a feature intervention experiment during the image generation process of Stable Diffusion v2 (Rombach et al., 2022).

Intervention. As shown in Figure 9, we investigate the generation process by intervening in modality-

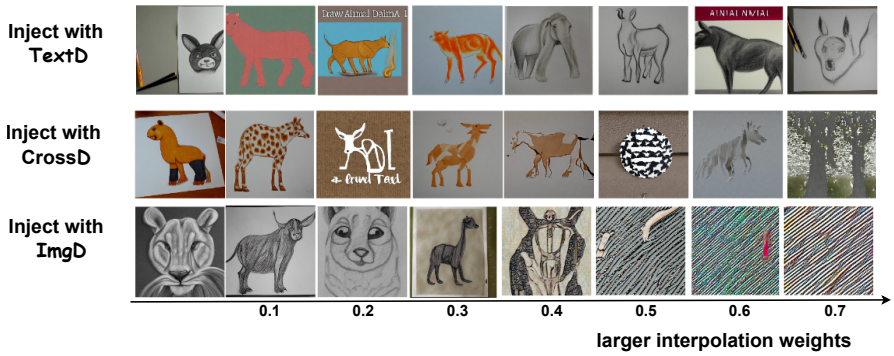

Figure 8: Generated new images from the VLM with the text prompt *"Please draw an animal"* and varying levels of intervention from a reference image (horse). From left to right, the interpolation weights α range from 0.0 to 0.7. Images generated with `TextD` typically depict clear main subjects (horse) without transferring the visual background details from the reference image. In contrast, injection of `ImgD` introduces low-level visual details as well as image distortions when α is large.

specific features in Stable-Diffusion-v2, which can be viewed as a VLM with an encoder and decoder (generator). The input text prompt is *"Please draw an animal"*. The encoder generates an embedding $\mathbf{T}$, representing the original multimodal embedding ready for generation. Additionally, we provide a reference image (here, a horse), processed by the same encoder, producing a reference embedding $\mathbf{R}$. To control the generation through modality-specific feature intervention, we interpolate $\mathbf{T}$ with $\mathbf{R}$ only at feature indices specified by the Modality Dominance Score (MDS). The resulting multimodal embedding is computed as: $\mathbf{T}'[I] = \alpha\mathbf{T}[I] + (1-\alpha)\mathbf{R}[I]$, where the interpolation is only applied to the index set I, corresponding to `TextD`, `CrossD`, and `ImgD` features.

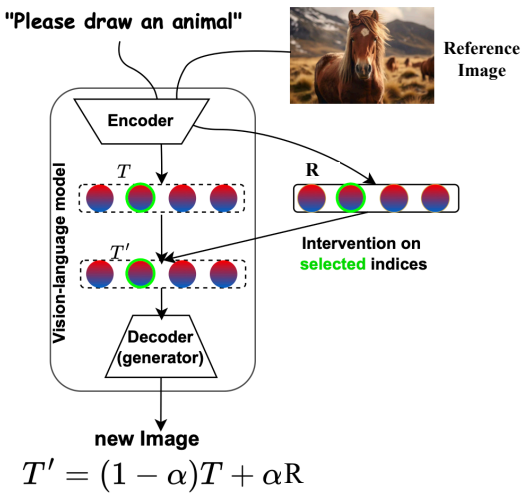

Figure 9: Controllable text-2-image generation via editing the modality-specific information from the reference image.

Results. We feed $\boldsymbol{T}'$ to the generator of the VLM with different α ranging from 0 to 0.7 with an interval of 0.1. The generated images with the selected indices correspond to `TextD`, `CrossD`, and `ImgD` are shown in Figure 8. The results clearly demonstrate that larger interventions on `TextD` lead to stronger control over high-level semantic concepts—for example, the generated image more distinctly resembles a horse (head). All these generated images injected by `TextD` typically depict clear main subjects without transferring visual background details from the reference image. In contrast, interventions on `ImgD` result in more visual details from the reference image being preserved, such as non-white and fur-like patterned background, which are visible in `ImgD` when $\alpha \geq 0.3$. To better contrast the effects of `ImgD` and `TextD`, we also use a reference image with a horse as the main subject, but in different styles/backgrounds. More results are shown in Figure A6.

6 Conclusion

In this study, we explored the monosemanticity of features within VLMs to elucidate the commonalities and distinctions across visual and linguistic modalities. Specifically, we successfully categorized multimodal features according to their dominant modality. Our proposed embedding-based interpretability metrics fill the gap in multimodal monosemanticity assessment. Moreover, we designed lightweight probing and editing methods based on modality-specific features and demonstrated great potential in mitigating gender bias, defending against adversarial attacks, and enabling controllable multimodal generation.

Limitation

While our work provides valuable insights into modality-specific feature analysis in vision-language models, several limitations warrant discussion. First, we did not conduct human studies to validate our interpretability metrics. Although our embedding-based metrics align with existing interpretability tools, direct human evaluation could provide stronger evidence that our categorizations match human cognitive interpretations of modality dominance. Second, our experiments focus exclusively on CLIP-family models. The generalizability of our findings to other vision-language architectures (e.g., BLIP or autoregressive VLMs) remains an open question. Different architectural designs may exhibit distinct modality gap characteristics that require adapted analysis methods.

References

Steven Bills, Nick Cammarata, Dan Mossing, Henk Tillman, Leo Gao, Gabriel Goh, Ilya Sutskever, Jan Leike, Jeff Wu, and William Saunders. 2023. Language models can explain neurons in language models. *URL https://openaipublic. blob. core. windows. net/neuron-explainer/paper/index. html.(Date accessed: 14.05. 2023)*, 2.

Xuanming Cui, Alejandro Aparcedo, Young Kyun Jang, and Ser-Nam Lim. 2024. On the robustness of large multimodal models against image adversarial attacks. In *Proceedings of the IEEE/CVF Conference on Computer Vision and Pattern Recognition*, pages 24625–24634.

Hoagy Cunningham, Aidan Ewart, Logan Riggs, R. Huben, and Lee Sharkey. 2023. Sparse autoencoders find highly interpretable features in language models. *International Conference on Learning Representations*.

DeepSeek-AI, Aixin Liu, and Bei Feng et al. 2024. Deepseek-v3 technical report. *Preprint*, arXiv:2412.19437.

Nelson Elhage, Neel Nanda, Catherine Olsson, and Others. A mathematical framework for transformer circuits. *Transformer Circuits Thread (2022)*.

Lingzhong Fan, Hai Li, Junjie Zhuo, Yu Zhang, Liangfu Chen, Zhengyi Yang, Congying Chu, Sangma Xie, Angela Laird, Peter Fox, Simon Eickhoff, Chunshui Yu, and Tianzi Jiang. 2016. The human brainnetome atlas: A new brain atlas based on connectional architecture. *Cerebral Cortex*, 26:bhw157.

Leo Gao, Tom Dupré la Tour, Henk Tillman, Gabriel Goh, Rajan Troll, Alec Radford, Ilya Sutskever, Jan Leike, and Jeffrey Wu. 2024. Scaling and evaluating sparse autoencoders. *arXiv preprint arXiv:2406.04093*.

Mor Geva, Roei Schuster, Jonathan Berant, and Omer Levy. 2021. Transformer feed-forward layers are key-value memories. In *Proceedings of the 2021 Conference on Empirical Methods in Natural Language Processing*, pages 5484–5495, Online and Punta Cana, Dominican Republic. Association for Computational Linguistics.

Wes Gurnee, Neel Nanda, Matthew Pauly, Katherine Harvey, Dmitrii Troitskii, and Dimitris Bertsimas. 2023. Finding neurons in a haystack: Case studies with sparse probing. *ArXiv*, abs/2305.01610.

Gabriel Ilharco, Mitchell Wortsman, Ross Wightman, Cade Gordon, Nicholas Carlini, Rohan Taori, Achal Dave, Vaishaal Shankar, Hongseok Namkoong, John Miller, Hannaneh Hajishirzi, Ali Farhadi, and Ludwig Schmidt. 2021. Openclip. If you use this software, please cite it as below.

Nicholas Jiang, Anish Kachinthaya, Suzanne Petryk, and Yossi Gandelsman. 2025. Interpreting and editing vision-language representations to mitigate hallucinations. In *The Thirteenth International Conference on Learning Representations*.

Wonjae Kim, Bokyung Son, and Ildoo Kim. 2021. Vilt: Vision-and-language transformer without convolution or region supervision. *arXiv preprint arXiv:2102.03334*.

Jing Yu Koh, Daniel Fried, and Russ R Salakhutdinov. 2024. Generating images with multimodal language models. *Advances in Neural Information Processing Systems*, 36.

Yangguang Li, Feng Liang, Lichen Zhao, Yufeng Cui, Wanli Ouyang, Jing Shao, Fengwei Yu, and Junjie Yan. 2022. Supervision exists everywhere: A data efficient contrastive language-image pre-training paradigm. In *International Conference on Learning Representations*.

Zhaowei Li, Wei Wang, YiQing Cai, Qi Xu, Pengyu Wang, Dong Zhang, Hang Song, Botian Jiang, Zhida Huang, and Tao Wang. 2025. Unifiedmllm: Enabling unified representation for multi-modal multi-tasks with large language model. In *Findings of the Association for Computational Linguistics: NAACL 2025*, pages 334–344.

Paul Pu Liang, Amir Zadeh, and Louis-Philippe Morency. 2024. Foundations & trends in multimodal machine learning: Principles, challenges, and open questions. *ACM Computing Surveys*, 56(10):1–42.

Weixin Liang, Yuhui Zhang, Yongchan Kwon, Serena Yeung, and James Zou. 2022. Mind the gap: Understanding the modality gap in multi-modal contrastive representation learning. In *Advances in Neural Information Processing Systems*.

Tom Lieberum, Senthooran Rajamanoharan, Arthur Conmy, Lewis Smith, Nicolas Sonnerat, Vikrant Varma, János Kramár, Anca Dragan, Rohin Shah, and Neel Nanda. 2024. Gemma scope: Open sparse

autoencoders everywhere all at once on gemma 2. *arXiv preprint arXiv:2408.05147*.

Tsung-Yi Lin, Michael Maire, Serge Belongie, James Hays, Pietro Perona, Deva Ramanan, Piotr Dollár, and C Lawrence Zitnick. 2014. Microsoft coco: Common objects in context. In *European conference on computer vision*, pages 740–755. Springer.

Haotian Liu, Chunyuan Li, Yuheng Li, and Yong Jae Lee. 2023. Improved baselines with visual instruction tuning.

Jiasen Lu, Dhruv Batra, Devi Parikh, and Stefan Lee. 2019. Vilbert: Pretraining task-agnostic visiolinguistic representations for vision-and-language tasks. In *Advances in Neural Information Processing Systems*, pages 13–23.

Jiquan Ngiam, Aditya Khosla, Mingyu Kim, Juhan Nam, Honglak Lee, and Andrew Y Ng. 2011. Multimodal deep learning. In *Proceedings of the 28th International Conference on Machine Learning (ICML-11)*, pages 689–696.

nostalgebraist. 2020. Interpreting gpt the logit lens. *https://www.lesswrong.com/posts/AcKRB8wDpdaN6v6ru/interpreting-gpt-the-logit-lens*.

Chris Olah, Nick Cammarata, Ludwig Schubert, Gabriel Goh, Michael Petrov, and Shan Carter. 2020. Zoom in: An introduction to circuits. *Distill*, 5(3):e00024–001.

Allan Paivio. 1991. Dual coding theory: Retrospect and current status. *Canadian Journal of Psychology/Revue canadienne de psychologie*, 45(3):255.

Letitia Parcalabescu and Anette Frank. 2023. Mm-shap: A performance-agnostic metric for measuring multimodal contributions in vision and language models & tasks. In *Proceedings of the 61st Annual Meeting of the Association for Computational Linguistics (Volume 1: Long Papers)*, pages 4032–4059.

Letitia Parcalabescu and Anette Frank. 2025. Do vision & language decoders use images and text equally? how self-consistent are their explanations? In *The Thirteenth International Conference on Learning Representations*.

Jayneel Parekh, Pegah Khayatan, Mustafa Shukor, Alasdair Newson, and Matthieu Cord. 2024. A concept-based explainability framework for large multimodal models. *Advances in Neural Information Processing Systems*, 37:135783–135818.

Anirudh Phukan, Divyansh, Harshit Kumar Morj, Vaishnavi, Apoorv Saxena, and Koustava Goswami. 2025. Beyond logit lens: Contextual embeddings for robust hallucination detection & grounding in VLMs. In *Proceedings of the 2025 Conference of the Nations of the Americas Chapter of the Association for Computational Linguistics: Human Language Technologies (Volume 1: Long Papers)*, pages 9661–9675, Albuquerque, New Mexico. Association for Computational Linguistics.

Alec Radford, Jong Wook Kim, Chris Hallacy, Aditya Ramesh, Gabriel Goh, Sandhini Agarwal, Girish Sastry, Amanda Askell, Pamela Mishkin, Jack Clark, and 1 others. 2021. Learning transferable visual models from natural language supervision. *arXiv preprint arXiv:2103.00020*.

Isha Rawal, Shantanu Jaiswal, Basura Fernando, and Cheston Tan. 2023. Dissecting multimodality in videoqa transformer models by impairing modality fusion. In *International Conference on Machine Learning*.

Robin Rombach, Andreas Blattmann, Dominik Lorenz, Patrick Esser, and Björn Ommer. 2022. High-resolution image synthesis with latent diffusion models. In *Proceedings of the IEEE/CVF Conference on Computer Vision and Pattern Recognition (CVPR)*, pages 10684–10695.

Simon Schrodi, David T. Hoffmann, Max Argus, Volker Fischer, and Thomas Brox. 2025. Two effects, one trigger: On the modality gap, object bias, and information imbalance in contrastive vision-language models. In *The Thirteenth International Conference on Learning Representations*.

Piyush Sharma, Nan Ding, Sebastian Goodman, and Radu Soricut. 2018. Conceptual captions: A cleaned, hypernymed, image alt-text dataset for automatic image captioning. In *Proceedings of ACL*.

Erfan Shayegani, Yue Dong, and Nael Abu-Ghazaleh. 2024. Jailbreak in pieces: Compositional adversarial attacks on multi-modal language models. In *The Twelfth International Conference on Learning Representations*.

Charles Spence. 2011. Crossmodal correspondences: A tutorial review. *Attention, Perception, & Psychophysics*, 73(4):971–995.

Zhiqing Sun, Sheng Shen, Shengcao Cao, Haotian Liu, Chunyuan Li, Yikang Shen, Chuang Gan, Liangyan Gui, Yu-Xiong Wang, Yiming Yang, and 1 others. 2024. Aligning large multimodal models with factually augmented rlhf. In *Findings of the Association for Computational Linguistics: ACL 2024*, pages 13088–13110.

Vinitra Swamy, Malika Satayeva, Jibril Frej, Thierry Bossy, Thijs Vogels, Martin Jaggi, Tanja Käser, and Mary-Anne Hartley. 2024. Multimodn—multimodal, multi-task, interpretable modular networks. *Advances in Neural Information Processing Systems*, 36.

Adly Templeton. 2024. *Scaling monosemanticity: Extracting interpretable features from claude 3 sonnet*. Anthropic.

Yifei Wang, Qi Zhang, Yaoyu Guo, and Yisen Wang. 2024. Non-negative contrastive learning. *ICLR*.

Hanqi Yan, Yanzheng Xiang, Guangyi Chen, Yifei Wang, Lin Gui, and Yulan He. 2024. Encourage or inhibit monosemanticity? revisit monosemanticity from a feature decorrelation perspective. *ArXiv*, abs/2406.17969.

Ziyi Yin, Muchao Ye, Tianrong Zhang, Tianyu Du, Jinguo Zhu, Han Liu, Jinghui Chen, Ting Wang, and Fenglong Ma. 2024. Vlattack: Multimodal adversarial attacks on vision-language tasks via pre-trained models. *Advances in Neural Information Processing Systems*, 36.

Jinghao Zhang, Guofan Liu, Qiang Liu, Shu Wu, and Liang Wang. 2024. Modality-balanced learning for multimedia recommendation. In *Proceedings of the 32nd ACM International Conference on Multimedia*, pages 7551–7560.

Yu Zhang, Jinlong Ma, Yongshuai Hou, Xuefeng Bai, Kehai Chen, Yang Xiang, Jun Yu, and Min Zhang. 2025. Evaluating and steering modality preferences in multimodal large language model. *arXiv preprint arXiv:2505.20977*.

A Appendix

A.1 Implementation of MDS

Based on the trained CLIP, CLIP+SAE, CLIP+NCL, and DeCLIP, we feed the test split of `cc3m-wds` dataset to these pretrained models, around 15k image-text pairs to calculate MDS, according to Eq.(1). The features are the last-layer output from the text and image encoder. We tried to calculate the normalization of z_i and z_t, but found that it makes little difference to the final results. It could be attributed to the existing normalization technique in image and text encoders in CLIP.

A.2 CrossD Qualitative Results

`CrossD` (the majority features) capture shared semantics across modalities. Different from modality-specific features, `TextD` and `ImgD`, `CrossD` features capture common concepts that could be expressed in both visual and language modalities. We randomly select two `CrossD` features and show their top-activated images and texts. As shown in Figure A1, Feature-6 mostly activates scenes involving individuals performing activities, especially outdoor activities, and feature-47 captures general outdoor environments. The coherence across both modalities reflects successful alignment, which is consistent with multimodal training objectives.

A.3 Implementation for Comparison Models

The three comparision models, DeCLIP, Multimodal SAE, and Multimodal NCL are all on top of the canonical ViT-B-32 CLIP [3] model from OpenAI (Radford et al., 2021), with ResNet50. The four methods (including CLIP) share the same model structures but are trained with different training objectives. We load them by feeding the checkpoints using the `open_clip.create_model_and_transforms` function in the published https://github.com/mlfoundations/open_clip.

The feature dimensions of the output features from the image encoder and text encoder are both 1024, the same for CLIP, DeCLIP, and Multimodal NCL. To retain the multimodal representation efficiency in downstream tasks, we have trained the SAE and NCL to reach a very small reconstruction loss for the original features z from CLIP. The dataset for NCL and SAE training is the train split (around 2900k image-text pairs) from `cc3m-wds`[4]. We train the two variants, i.e., SAE and NCL, on top of the pretrained CLIP using a single 3090 GPU.

DeCLIP. We use the checkpoint released in https://github.com/Sense-GVT/DeCLIP to extract the last layer features, z_i and z_t.

Multimodal SAE. We insert an SAE model to map the original feature into a sparse latent space, i.e., $z^d \rightarrow z^n$, with top-k latent as nonzero values. Empirically, we found that when $n = d$ and $k = 32$, we can get the best results to balance the sparsity and downstream task performance. Such an SAE model (shared parameter) is inserted at the end of the image and text encoder in CLIP.

```
def get_sae_embedding(self, z):
    z = self.encoder(z)
    z_sae = F.relu(z)
    vals, ids = z_sae.topk(self.k, dim=1)
    z_sae = torch.zeros_like(z_sae)
    z_sae.scatter_(1, ids, vals)
    return z_sae
```

Inspired by (Gao et al., 2024), we train the SAE until the sparsity (the inactive dimension) of image features and text features doesn't increase (the same stop criteria for NCL). Noting that there are many zero values in z^{sae}, we remove those zero activity features (called dead latents in (Gao et al., 2024)) for further studies. We show the changes of active dimensions of image features and text features in Figure A2.

Non-negative Contrastive Learning (NCL). We add the NCL block, i.e., the projector, after obtaining z_i and z_t from the image encoder and text encoder. The training loss is shown in Eq. 3.

```
self.projector = nn.Sequential(
    nn.Linear(embed_dim, embed_dim),
    nn.LayerNorm(embed_dim),
    nn.ReLU(),
    nn.Linear(embed_dim, embed_dim),
)
z_ncl = self.projector(z)
```

Similarly, the activated dimensions for image features and text features decrease and are then flattened (shown in Figure A3.) By comparing with Figure A2, we noticed that the features in SAE is much more sparse than those in NCL.

[3] https://github.com/openai/CLIP

[4] https://huggingface.co/datasets/pixparse/cc3m-wds

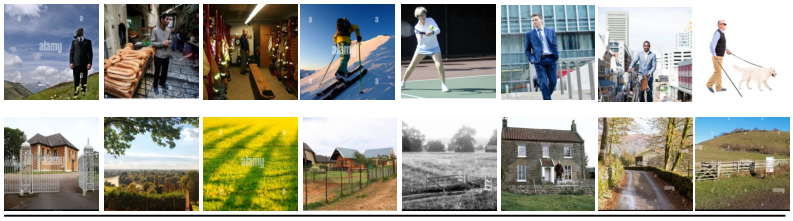

Feature-6: Actions performed by individuals	*Feature-47: Outdoors Scenery*
Young man working on invention in a warehouse.	A stile on a public footpath overlooking the village on a frosty autumn morning.
cricketers exercise during a practice session.	A private chapel, and the wrought iron gates in the grounds.
Cricket player checks his bat during a training session.	Train track: a man blending in with the scenery as he stands on a railway track near a river
Basketball coach watches an offensive possession from the sideline during the second half.	surveying the scene: people look out over loch today on a warm day in the village

Figure A1: Activated images and texts by `CrossD` features. Top image row (feature 6): activities performed by individuals. Bottom image row (feature 47): scenery outside the doors. Text in blue aligns with visual concepts.

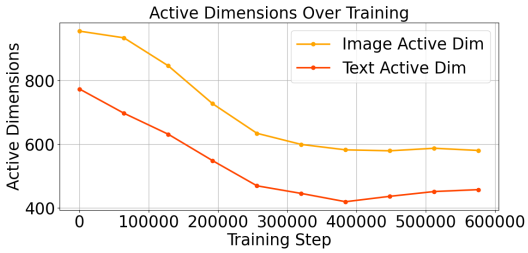

Figure A2: The changes of active dimensions over **SAE** training.

Figure A3: The changes of active dimensions over **NCL** training.

A.4 Interpretability Evaluation

A.4.1 Implementation

Embedding models h for activated image/text samples. Our interpretability metrics, i.e., ***EmbSim*** and ***WinRate*** are based on the embeddings of active image/text samples by each feature. We need the embedding models to obtain these embeddings, i.e., Z^+ and Z^-. We use the Vision Transformer (ViT-B-16-224-in21k) for image embeddings and the Sentence Transformer (all-MiniLM-L6-v2) for text embeddings. The goal here is to derive the general and effective image and text embeddings, so we can also use the image encoder and text encoder from CLIP.

A.4.2 Results

MDS for different methods MDS with monosemanticity enhancements. With the monosemanticity-improving models (SAE and NCL), we hypothesize that modality purity will become more pronounced, making dominant modality assignments more meaningful. To validate this, we calculate the MDS and visualize the distributions of the three feature groups across models in Figure A4. Interestingly, we find that CLIP, which is only trained on an image-text contrastive learning objective, contains a spectrum of features with different modality dominance. Specifically, its distribution skews towards the image modality, and this trend is consistent across all models. DeCLIP, on the other hand, shows a more balanced and less centered distribution. This suggests that DeCLIP, through self-supervision, extracts more modality-specific features, which might be overlooked by pure vision-language contrastive models like CLIP. The extracted features on top of NCL and SAE also exhibit less skewness, with SAE showing the most balanced distribution, indicating its strong capability to extract diverse monosemantic features.

EmbSimi and WinRate for Monosemanticity measurement. Firstly, we show the complete results for ***EmbSmi*** and ***WinRate*** in the Table A1.

The results of monosemanticity changes as training goes on. We show the results of monosemanticity score changes as training goes on for both

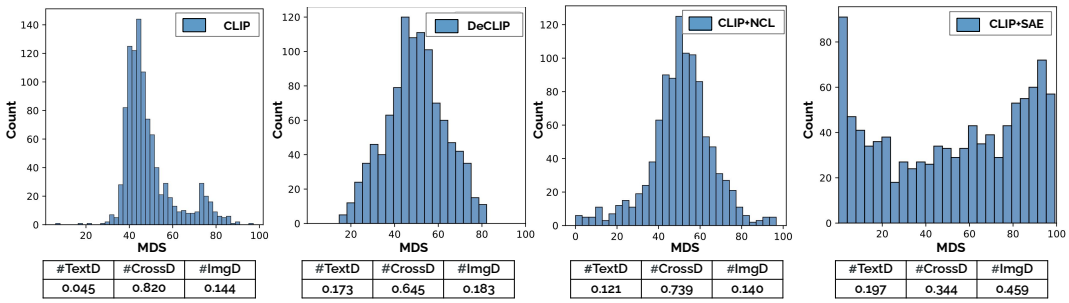

Figure A4: Modality Dominance Score (MDS) distributions of three feature categories for different VLMs.

Models	***EmbSim***		***WinRate***	
Activated→	Image	Text	Image	Text
CLIP	0.11	0.45	0.65	0.59
DeCLIP	0.06	-0.07	0.61	0.46
CLIP+NCL	0.14	0.45	**0.71**	0.60
CLIP+SAE	**0.17**	**0.74**	0.60	**0.61**

Table A1: Average interpretability scores (by examining the top activated images/texts) for features extracted from VLMs.

Models	**CLIP**	**DeCLIP**	**CLIP+NCL**	**CLIP+SAE**
Mono* is *EmbSim				
Visual Mono	-0.007	0.009	**0.043**	0.005
Textual Mono	-0.017	-0.001	**0.210**	0.146
Mono* is *WinRate				
Visual Mono	-0.007	0.005	0.002	**0.030**
Textual Mono	-0.069	-0.059	**0.018**	0.016

Table A2: The visual and textual monosemanticity. A higher value indicates that `ImgD` captures more visual than linguistic features, and vice versa for `TextD`.

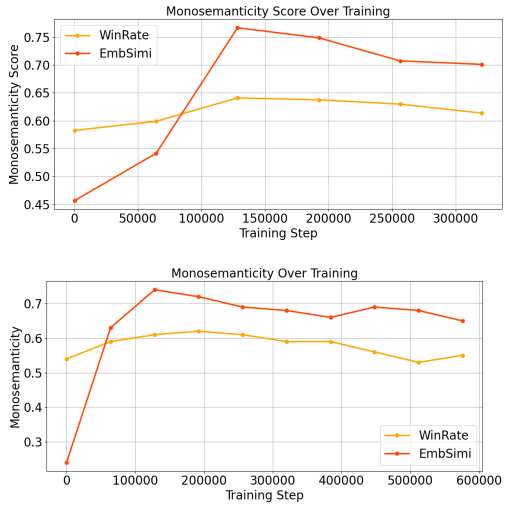

Figure A5: Monosemanticity (EmbSimi and WinRate) changes as training goes on. Upper is for CLIP+NCL, bottom is for CLIP+SAE.

NCL and SAE in Figure A5.

A.5 Implementations and More Results for Case Studies

We provide the implementation details and more experimental results for the three case studies in the following.

A.5.1 Understanding Gender Patterns

Datasets. We select male and female images using a gender classifier touchtech/fashion-images-gender-age-vit-large-patch16-224-in21k-v3 from cc3m-wds validation set. We have both input images and text; the original gender classification accuracy is 83.4% and 73.4%, respectively.

Classification. As the intervened features are not compatible with existing pretrained text or text classifiers, we compare these features with the golden feature from male and female data. Specifically, we randomly select a female/male image with classification logits larger than 0.9 (ensuring the gender patterns are obvious) as the reference features. We use the same embedding models in §A.4, i.e., Vision Transformer and Sentence Transformer as the encoder and encode both intervened feature and golden feature. The intervened feature is labeled with the same label as the reference image, for which its distance in encoder space is smaller.

Intervention. There are different number of `ImgD` and `TextD` for a given representation of input sample. To avoid the effects of different numbers of removal features, we remove (set the corresponding dimension as zero) the minimal number between `ImgD` and `TextD`, and remove the same number of randomly selected features as a baseline.

`TextD` in male concepts. We also cluster different male descriptions according to the percentage of `TextD` features among all their top-20 activated features, and we calculate the frequency of the top7 tokens in each cluster shown in Table A3. We remove the gendered personal pronouns, e.g., he,

she, woman, man, boy, girl, and only focus on how gender-neutral concepts represent the gender. With more TextD injection, the textual descriptions become more sports-related, such as coach, basketball, soccer; while the sentences with less activated TextD have top words, such as party, hip, game, smile, home. This trend is consistent with the social stereotype that males are more active in sports activities.

A.5.2 Defense against Adversarial Attacks

Models We employed the same ViT-B-32 CLIP as in §A.3 as the multimodality feature extractor shown in the Figure 7 to extract 1024-dimension features, so we use the categorized TextD, ImgD and CrossD calculated before. We use LLaVA-1.5-7b as the attacked VLM (Liu et al., 2023). The whole process of defensing adversarial attacks is two steps:

- **Generating adversarial images by injecting harmful requests.** We have a benign scenery image and a list of 50 harmful requests. Firstly, we create an image with a white background with the text saying the one piece of harmful request, as the contrast image. Then, we apply the alignment training by minimizing the distance between the benign image and the contrast image in the embedding space of the image encoder. The benign image is thus being injected with harmful semantics, denoted as $\mathbf{F}_{adv}$.

- **Defending the adversarial attacks.** To remove the toxicity of the adversarial samples, we employ the alignment training shown in Figure 7 by updating the embeddings of the adversarial samples. Specifically, we only select the target features, i.e., the ImgD, TextD, and CrossD to be involved in the training.

When attacking the VLM, we feed the adversarial images/samples along with the text prompt, i.e., the corresponding harmful request injected into the adversarial sample. For each adversarial sample, we repeat the attack process 100 times. For comparison, we apply the original generated 50 adversarial samples to attack VLM, and the average success rate is 73.26%; and the success rate of the (benign image - harmful request) is 10.00%. We conducted five independent runs for each experiment to ensure statistical reliability. Results in the tables show mean values across runs, with relative standard deviations below 3% for accuracy metrics.

Computing resources cost The experiments were conducted with a GPU with 48GB of memory. Adversarial sample generation requires approximately 4 GPU hours, while adversarial sample detoxification takes approximately 6 GPU hours.

A.5.3 Controllable Text-to-Image Generation

Models. We select Stable-Diffusion-v2 (https://huggingface.co/stabilityai/stable-diffusion-2) as our text-2-image generation model. As its image encoder (CLIP-ViT-H-14-laion2B-s32B-b79K) is not the same CLIP we used before, we recalculate the MDS distribution to derive the three categories of features.

More results. We present additional images generated by modifying the original multimodal representation through feature injection from a reference image. To emphasize the distinction between ImgD and TextD, we use two reference images of horses in different backgrounds and artistic styles. Specifically, we compare two sets of images where features from sketch and oil painting styles are injected using ImgD. We observe that images influenced by sketches tend to be predominantly black and white, while those influenced by oil paintings appear more colorful. In contrast, the images generated using TextD remain visually similar across both the sketch and oil painting settings.

Percentage of `TextD`	Top8 words in male-related textual description
0.1	attends, party, hip, game, comedian, city, black, artist
0.12	smile, made, blue, outside, looks, home, got, book
0.18	artist, player, film, pop, performs, festival, young, suit
0.24	player, football, basketball, team, game, portrait, holding, gym

Table A3: Representative words in male-related descriptions with different percentages of `TextD`.

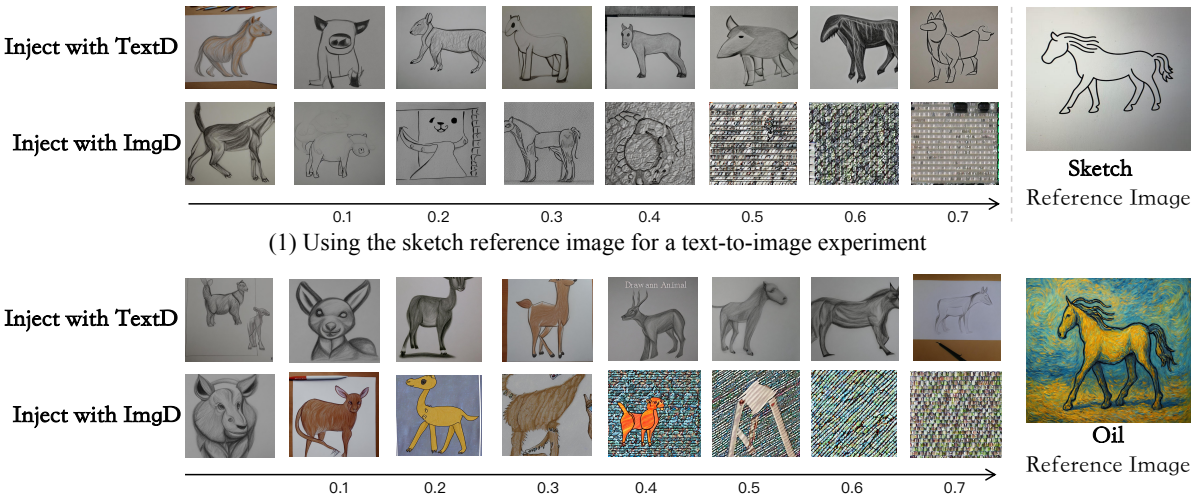

(1) Using the sketch reference image for a text-to-image experiment

(2) Using the oil reference image for a text-to-image experiment

Figure A6: Generated new images from the VLM with the text prompt *"Please draw an animal"* and varying levels of intervention from different reference images. We found that *TextD* captures significant semantic information, such as shape, etc. Notably, when a sketch is selected as the reference image, both *imgD* and *TextD* display sketch-like stylistic features. When oil-painting is chosen as the reference image, both *imgD* and *TextD* exhibit styles that resemble oil paintings. Comparatively, the stylistic differences between *imgD* in conditions (1) and (2) are distinct: *imgD* in (1) lacks color, whereas *imgD* in (2) presents diverse coloration. Similar to Figure 8, *TextD* does not affect low-level visual features, while *ImgD* shows significant distortion at higher α values.